Jpn. J. Appl. Phys. Vol. 35 (1996) pp. 2061–2067
Part 1, No. 4A, April 1996

# Effect of Fermi Level Motion on the Optical, ESR and Transport Properties of $CuInSe_2$

Katsuaki SATO, Nobuyuki NISHIKAWA*[1], Igor AKSENOV*[2], Takeshi SHINZATO and Hisayuki NAKANISHI[1]
*Faculty of Technology, Tokyo University of Agriculture and Technology, Koganei, Tokyo 184, Japan*
[1] *Faculty of Science and Technology, Science University of Tokyo, Noda, Chiba 278, Japan*

(Received December 20, 1995; accepted for publication January 31, 1996)

The infrared (IR) absorption and ESR spectra of the $CuInSe_2$ crystals, grown by the normal freezing technique and subsequently annealed in various atmospheres, have been studied in connection with the annealing-induced motion of the Fermi level relative to the energy band edges. The degenerate n-type crystals exhibited a free-electron absorption, while the p-type crystals showed both an inter-valence-band and a free-hole absorption, from the analysis of which the energy positions of the Fermi level have been evaluated, and the electrical parameters of the respective crystals estimated; these results were then compared with the experimental results. In the ESR spectra the signals from iron residual impurity in both divalent and trivalent charged states, as well as the signals arising from native defects $V_{Cu}$ and $In_{Cu}$, have been detected, the intensities of the ESR signals being dependent on the composition of the samples and the Fermi level position.

KEYWORDS: $CuInSe_2$, inter-valence-band absorption, free-carrier absorption, Fe impurity, ESR, Fermi level

## 1. Introduction

Ternary chalcopyrite-type semiconductor $CuInSe_2$ has been extensively studied as a very promising material for solar cell applications because of its high optical absorption coefficient ($\alpha > 10^4$ cm$^{-1}$ ) and favorable direct band gap ($E_g = 1.08$ eV),[1] as well as its versatile optical and electrical properties which can, in principle, be tuned for the specific needs of a particular device structure.

In order to realize the tuning of the characteristics of $CuInSe_2$ it is vital to know the dependence of the electrooptical properties of this material on the Fermi level in relation to the band edges, since the position of the Fermi level determines the physical properties of semiconductors, i.e., the conductivity type and carrier concentrations, as well as the charged states of deep centers, including those formed by residual transition atom ions.[2] The position of the Fermi level relative to the band edges can be influenced by thermal treatments of the material due to the annealing-induced changes in the material stoichiometry, as well as changes in the concentrations of intrinsic and extrinsic defects.

In this study we report the results of infrared (IR) optical absorption and electron spin resonance (ESR) investigations of $CuInSe_2$ single crystals in connection with the annealing-induced motion of the Fermi level relative to the band edges of $CuInSe_2$.

## 2. Experimental

Single crystals of $CuInSe_2$ were grown by the normal freezing method at Science University of Tokyo. The constituent elements (Cu, In, and Se of 99.9999% purity) were heated to 1150°C with subsequent slow cooling at the rate of 5°C/h; the details have been published elsewhere.[3] Thermal annealing of the crystals in vacuum, Se-vapor and in the presence of Cu was carried out for 50 h at 650°C.

The obtained crystals were characterized by the thermal probe and four-probe methods to determine their conductivity type and resistivities, respectively, as well as by electron probe microanalysis (EPMA) to determine their composition using a JEOL type JXA-8900 microanalyzer. In some of the low resistivity p-type and n-type crystals, the Hall mobilities were measured by the van der Pauw technique. Hall data could be obtained only in a limited number of crystals since some of the samples measured were too small to obtain good electrical contacts.

Optical absorption measurements were carried out at room temperature (RT) using a BOMEM Type MB100 Fourier Transform IR spectrometer with a focusing attachment to ensure the optical beam diameter of about 2 mm. ESR spectra were taken at 4.2 K with a JEOL JES-RE2X X-band spectrometer with the microwave power of 5 mW.

## 3. Results and Discussion

### 3.1 *Sample characterization*

The composition and electrical properties of the $CuInSe_2$ crystals—as-grown and annealed in various atmospheres—are shown in Table I.

It can be seen that the as-grown and Se-vapor-annealed samples become highly conductive p-type, whereas annealing in vacuum or in the presence of Cu renders them highly conductive or semi-insulating n-type, respectively. On the basis of EPMA results and taking into account the defect chemistry model of ternary compounds,[4] the deviation of the actual composition of our samples from the ideal formula $CuInSe_2$ has been described by two parameters, $\Delta x = [Cu]/[In] - 1$ and $\Delta y = 2[Se]/([Cu] + 3[In]) - 1$ (where [ ] is the total concentration of respective atoms in the sample), which determine the deviation from molecularity and valence stoichiometry, respectively.

Analysis of the parameters $\Delta x$ and $\Delta y$ combined with the data on the formation energies of the defects in $CuInSe_2$[5] allows us to determine the most probable native defects in the as-grown and annealed crystals. These majority defects are also shown in Table I. From these

*[1]Present address: Fujitsu Corporation Ltd., Kamikotanaka, Kawasaki, Kanagawa 211, Japan.
*[2]Present address: Electrotechnical Laboratory, Umezono, Tsukuba 305, Japan.

Table I. Annealing-induced changes in the composition and electrical properties of $CuInSe_2$ crystals together with the electrically active native defects with the lowest formation energies likely to be formed due to deviations from molecularity ($\Delta x \neq 0$) and valence stoichiometry ($\Delta y \neq 0$). The underlined defects have been detected by ESR.

| Samples | As-grown | Vacuum annealed | Cu-vapor annealed | Se-vapor annealed |
|---|---|---|---|---|
| Conduction type | p | n | n | p |
| Resistivity ($\Omega$cm) | $10^{-1}$ | 1 | $10^{-3}$ | $10^{-1}$ |
| Cu (at.%) | 26 | 25 | 29 | 23 |
| In (at.%) | 24 | 28 | 26 | 25 |
| Se (at.%) | 50 | 47 | 45 | 52 |
| $\Delta x$ (molecularity) | $>0$ | $<0$ | $>0$ | $<0$ |
| $\Delta y$ (stoichiometry) | $\sim 0$ | $<0$ | $<0$ | $>0$ |
| Majority defect | $V_{In}$, $Cu_{In}$ | $\underline{V_{Cu}}$, $\underline{In_{Cu}}$, $V_{Se}$ | $V_{In}$, $Cu_{In}$, $V_{Se}$ | $\underline{V_{Cu}}$, $\underline{In_{Cu}}$ |
| Formation energy (eV) | 2.8, 1.5 | 2.6, 1.4, 2.4 | 2.8, 1.5, 2.4 | 2.6, 1.4 |

native defects, expected from the defect chemistry considerations, we were able to identify two defects, namely, $V_{Cu}$ and $In_{Cu}$, from the ESR spectra discussed below.

Hall effect measurements in p-type and n-type crystals provided the hole mobility of 26 $cm^2/Vs$ on average and the electron mobility of 380 $cm^2/Vs$, which are in the range of those previously reported for $CuInSe_2$.[5] Carrier concentrations differed from sample to sample, the typical values being $\sim 3\times10^{18}$ $cm^{-3}$ and $3.5\times10^{18}$ $cm^{-3}$ for p-type and n-type crystals, respectively. No reliable data were obtained in high-resistivity crystals. The samples in which these transport data were evaluated do not necessarily correspond to those used to obtain the optical spectra.

### 3.2 *IR absorption*

#### 3.2.1 *General observations*

The typical IR absorption spectra of the as-grown and annealed $CuInSe_2$ crystals are shown in Fig. 1. The as-grown samples exhibit a broad absorption (A-band) peak at about 3000 $cm^{-1}$ (0.36 eV), which was found to be quenched by annealing in vacuum or in the presence of Cu. Annealing in Se-vapor, on the other hand, results in an enhancement of the A-band, as well as in an appearance of a new absorption (B-band) peak at lower energy ($1200\,cm^{-1} = 0.14$ eV).

Since the A- and B-bands were observed only in the highly conductive p-type samples, and by analogy with the results of the IR absorption studies of Ge [6] and GaAs,[7] we consider that these bands originate from inter-valence-band transitions between subbands of the valence band of $CuInSe_2$, split by the noncubic crystal field and the spin-orbit interaction. Existence of inter-valence-band IR absorption around 0.3 eV in $CuInSe_2$ has already been discussed by Neumann *et al.*[8]

The sharp rise of absorption at the low-energy side of the spectra, shown in Fig. 1, can be attributed to the free-carrier absorption, which is known to be observable in semiconductors at sufficiently high carrier concentrations.[9] Indeed, we could not observe this absorption in the semi-insulating samples (Cu-annealed) due to the low concentration of free carriers in those samples.

The IR absorption spectra of the as-grown (p-type) and vacuum-annealed (highly conductive n-type)

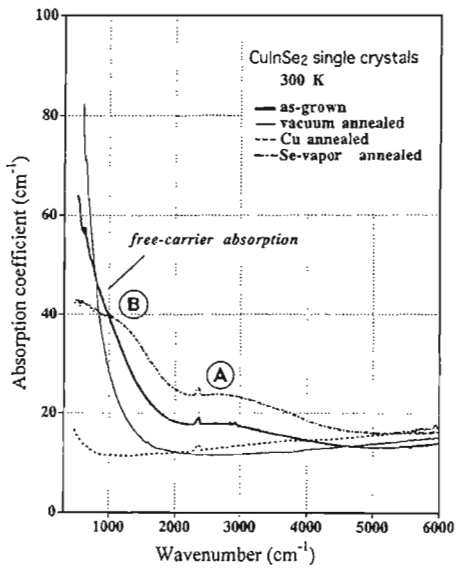


Fig. 1. IR absorption spectra of the $CuInSe_2$ crystals: as-grown (——) and annealed in vacuum (— — —), in the presence of Cu (- - - -) and in Se-vapor (– – – –)

$CuInSe_2$ crystals are shown in Figs. 2(a) and 2(b), respectively. Spectra of computer fits for the free-hole (p-type) and free-electron (n-type) absorptions are plotted as dotted curves in the figures. In the inset of Fig. 2(a), the difference between the experimentally measured absorption and that calculated for the free-carrier absorption is shown, which is suspected to originate from the inter-valence-band absorption.

For the vacuum-annealed samples we have also been able to observe an annealing-induced shift of the fundamental band-to-band absorption (Burstein-Moss shift) from $E_g = 0.95$ eV (original band gap) to $E_g' = 0.96$ eV (the spectra are not shown), attributed to an upward shift of the Fermi level, with the resulting Fermi level position being situated above the bottom of the conduction band, as schematically illustrated in Fig. 3(a). Therefore, the electrons in the conduction band of the vacuum-annealed samples are degenerate, which is expected to be easily achieved owing to the low value of the effective mass $m_e$ of the electrons in $CuInSe_2$ ($m_e = 0.09m_o$, where $m_o$ is the free-electron mass),[5] implying a sharp

curvature of the conduction band and a low density of states near its bottom.

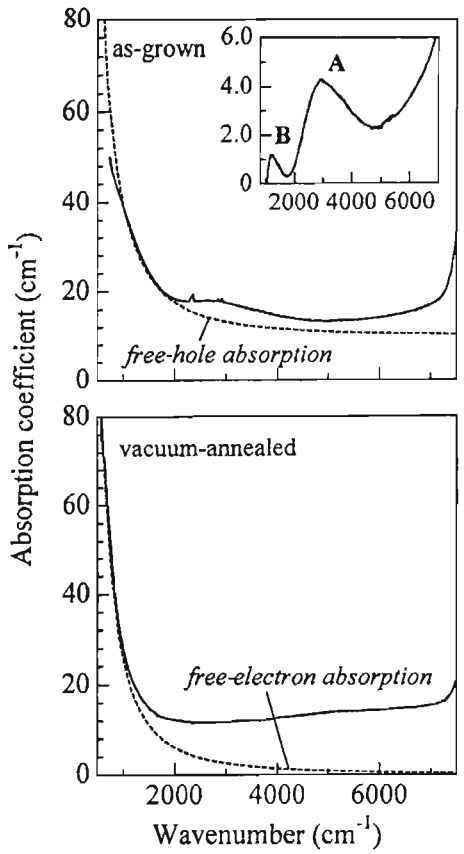


Fig. 2. IR absorption spectra of the as-grown (a) and vacuum-annealed (b) crystals together with computer fits for the free-carrier absorption. In the inset of (a) the difference between the experimentally measured absorption coefficient and that calculated for the free-carrier absorption, is shown. This difference represents the inter-valence-band absorption spectrum.

In a degenerate n-type semiconductor, the optical band gap $E_g'$ is given by a separation between the lowest unfilled level in the conduction band $E_{en}$ lying approximately at $4k_BT$ below the Fermi level $E_{fn}$, and the corresponding level $E_{hn}$ in the valence band lying $(m_e/m_h)(E_{en}-E_c)$ below the top of the valence band.[10] The shift of the fundamental absorption edge is then given by

$$\Delta E_g = E_g' - E_g = \left(1+\frac{m_e}{m_h}\right)(E_{fn}-E_c-4k_BT), \quad (1)$$

where $m_e/m_h$ takes into account the momentum conservation during optical transition.

Using the observed shift ($\Delta E_g = 10$ meV) and the reported effective mass values of electrons and holes, i.e., $m_e = 0.09m_o$ and $m_{hh} = 0.71m_o$,[5] the Fermi level $E_{fn}$ in the vacuum-annealed sample is determined to lie $4k_BT + 9$ meV ($= 109$ meV) above the bottom of the conduction band at RT. The optical band-to-band transitions then occur between the lowest unfilled level $E_{en}$ in the conduction band positioned $\sim 9$ meV above the conduction band bottom (see Fig. 3(a)) and the corresponding level in the valence band $E_{hn}$, which satisfies the momentum conservation rule (vertical electronic transition) and lies about 1 meV below the top of the valence band.

3.2.2 *Inter-valence-band absorption*

The energy band structure of $CuInSe_2$ relevant to this section is shown in Fig. 3(c). By the effect of the non-cubic crystal field ($\Delta_{cf}$) combined with the spin-orbit interaction ($\Delta_{so}$) the $\Gamma_{15}$ uppermost valence band of the zincblende structure is split into three components having the symmetry $\Gamma_6^5$, $\Gamma_7^4$ and $\Gamma_7^5$, where the upper indices indicate the single-group representation from which the double-group representation shown by lower indices originates. The positions of the $\Gamma_7^4$ and $\Gamma_7^5$ energy levels relative to that of the uppermost $\Gamma_6^5$ level are given by[5]

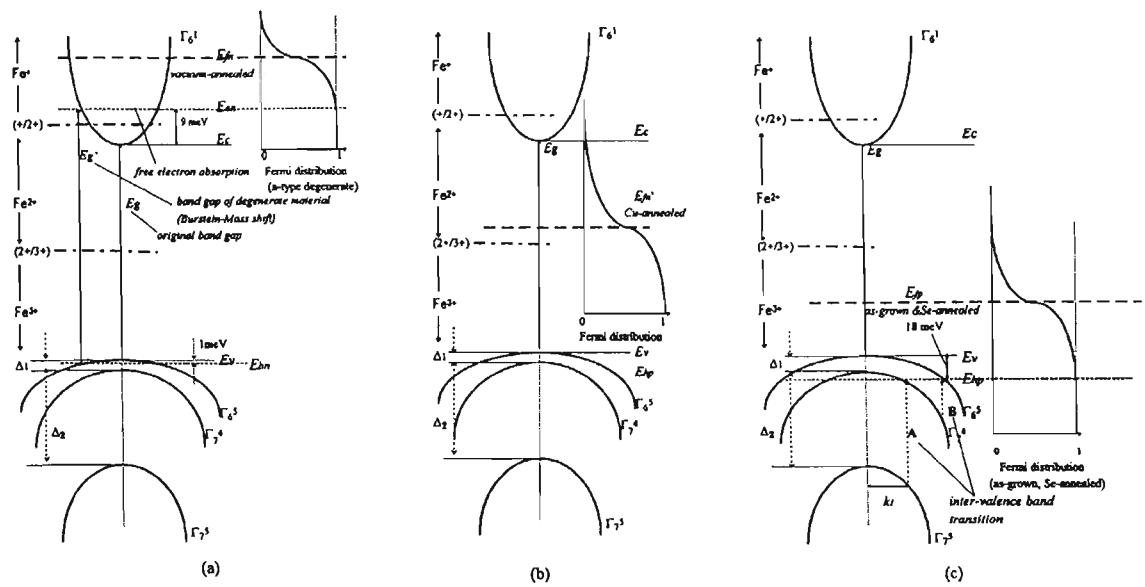


Fig. 3. The energy level diagram, showing the band structure of $CuInSe_2$ in the vicinity of the center of the first Brillouin zone for (a) vacuum-annealed n-type, (b) Cu-annealed n-type and (c) as-grown or Se-annealed p-type crystals. $E_{fn}$, $E_{fn}'$ and $E_{fp}$ (— — —) denote the Fermi level positions evaluated from the optical and ESR measurements. The lines (— – — – —) delineating iron in various charged states (*e.g.*, 2+/3+) show the demarcation levels of the Fe impurity. See text for details.

$$E(\Gamma_7^4) - E(\Gamma_6^5) = \Delta_1 = -\frac{1}{2}(\Delta_{cf} + \Delta_{so}) + \frac{1}{2}\left[(\Delta_{cf} + \Delta_{so})^2 - \frac{8}{3}\Delta_{cf}\Delta_{so}\right]^{1/2},$$

$$E(\Gamma_7^5) - E(\Gamma_6^5) = \Delta_2 = -\frac{1}{2}(\Delta_{cf} + \Delta_{so}) - \frac{1}{2}\left[(\Delta_{cf} + \Delta_{so})^2 - \frac{8}{3}\Delta_{cf}\Delta_{so}\right]^{1/2} \quad (2)$$

where $\Delta_{cf} = 0.006$ eV and $\Delta_{so} = 0.233$ eV.

The values of $\Delta_1$ and $\Delta_2$, evaluated from eq. (2) are 0.003 eV and 0.236 eV, respectively. The crystal-field splitting of the valence band in $CuInSe_2$ is very small, which is a result of a very small tetragonal distortion of the $CuInSe_2$ crystal lattice ($c/a = 2.007$).[11]

Since the momentum of a photon is negligible compared with the crystal momentum (the momentum of a carrier in an energy band), the momentum of the electron should be conserved in the photoabsorption process. The electron will thus undergo the vertical transition on the energy level diagram, shown in Fig. 3(c), with the initial state and the final state having the same momentum $k_1$. In the parabolic energy bands approximation, which is clearly the case in $CuInSe_2$,[5] we can write, for the absorption A-band, that

$$E_{hp} = \frac{\hbar^2 k_1^2}{2m_{hh}}, \quad (3)$$

$$E_A = \Delta_1 + \Delta_2 - E_{hp} + \frac{\hbar^2 k_1^2}{2m_{sh}}, \quad (4)$$

where $E_{hp}$ is the energy of the lowest unfilled level in the valence band for the p-type crystals (the energy of the final state of the electron transition), and $m_{hh}$ and $m_{sh}$ are the effective masses of holes in the respective valence subbands (see Fig. 3(c)). From eqs. (3) and (4) the following equation is derived;

$$E_A - (\Delta_1 + \Delta_2) = \frac{\hbar^2 k_1^2}{2}\left(\frac{1}{m_{sh}} - \frac{1}{m_{hh}}\right) = \frac{\hbar^2 k_1^2}{2m_{hh}}\left(\frac{m_{hh}}{m_{sh}} - 1\right) = E_{hp}\left(\frac{m_{hh}}{m_{sh}} - 1\right) \quad (5)$$

Using the observed transition energy $E_A = 0.36$ eV and reported values of effective mass, $m_{hh} = 0.71m_o$ and $m_{sh} = 0.085m_o$,[5] we can determine the energy position of level $E_{hp}$ inside the valence band as 16 meV. Now, given the position of the final state of the inter-valence-band transitions, we can predict that the transition between $\Gamma_7^4$ and $\Gamma_6^5$ valence subbands should take place at

$$E_B = \Delta_1 + \frac{\hbar^2 {k_1}^2}{2m_{lh}} - \frac{\hbar^2 {k_1}^2}{2m_{hh}} = \Delta_1 + E_{hp}\left(\frac{m_{hh}}{m_{lh}} - 1\right). \quad (6)$$

Applying $m_{lh} = 0.092m_o$ to eq. (6), we find the transition energy to be 0.14 eV ($\sim 1130\,cm^{-1}$), which is exactly the spectral position of the peak of the B-band shown in Fig. 1.

We, therefore, attribute the experimentally observed A- and B-bands in the IR absorption spectra of the p-type crystals to the transitions from the $\Gamma_7^5$ and $\Gamma_7^4$ valence subbands to the $\Gamma_6^5$ valence subband (see Fig. 3). Since the level $E_{hp}$ lies about $4k_BT$ (~100 meV) below the Fermi level for the p-type samples, we can determine the Fermi level position for the p-type samples as being $E_{fp} = 4k_BT - E_{hp} \sim 84$ meV above the top of the valence band. The Fermi level, therefore, lies in the band gap, i.e., the p-type crystal is nondegenerate.

3.2.3 *Free-carrier absorption*

As was discussed in §3.2.1, from the optical absorption measurements near the band edge it was found that the Fermi level in our highly conductive degenerate n-type samples lies about 109 meV above the bottom of the conduction band. Knowing the position of the Fermi level in the degenerate parabolic conduction band, as well as the electron effective mass, we can estimate the electron concentration in these samples at RT using the expression[12]

$$n_e = 4\pi\left(\frac{2m_e}{\hbar^2}\right)^{3/2}\int_{E_c}^{\infty}\frac{E^{1/2}}{1 + \exp\left(\frac{E - E_f}{k_BT}\right)}, \quad (7)$$

to be $n_e \sim 7 \times 10^{18}\,cm^{-3}$. This value is relatively close to the value of $3.5 \times 10^{18}\,cm^{-3}$ determined by the Hall measurement.

For the concentration of holes in the p-type samples, which are nondegenerate, we can write

$$n_p = 2\left(\frac{2\pi m_h k_B T}{\hbar^2}\right)^{3/2}\exp\left(\frac{E_v - E_f}{k_BT}\right), \quad (8)$$

where we introduced the effective density of states hole mass $m_h = (m_{hh}^{3/2} + m_{lh}^{3/2})^{2/3} = 0.73m_o$, since both heavy-hole and light-hole bands are considered to be equally populated at the temperature used in our experiment since $k_BT$ (~25 meV) greatly exceeds the value of $\Delta_1 = 3$ meV. From eq. (8) we obtain the RT concentration of holes in our p-type samples as $n_p \sim 5.6 \times 10^{17}\,cm^{-3}$. This value is about one order of magnitude smaller than the typical hole concentration of as-grown p-type crystals obtained from the Hall effect, $3 \times 10^{18}\,cm^{-3}$.

Given the concentrations of carriers in the respective energy bands, we can calculate the free-carrier absorption coefficient $\alpha_f$ using the classical (Drude) formula as applied to the degenerate energy bands in the first approximation[13]

$$\alpha_f = \frac{\omega_p^2\tau}{n_o c\epsilon_o}\frac{1}{(\omega\tau)^j + 1}, \quad (9)$$

where $n_o$ is the index of refraction, $\tau$ is the carrier relaxation time, $j$ is the fitting parameter and $\omega_p = (n_i e^2/m_i\epsilon_o)^{1/2}$ is the plasma frequency with $n_i$ and $m_i$ ($i$=e, h) being the concentrations and effective masses of the carriers in respective energy bands. Figure 2 shows the best fits of $\alpha_f$, given by eq. (9), to the experimental IR absorption spectra for the degenerate p-type (as-grown) and n-type (vacuum-annealed) $CuInSe_2$ crystals. From these computer fits we deduced the values of the fitting parameter $j$ and the carrier relaxation times for elec-

trons and holes as being $j_e = 2.139$, $\tau_e = 3.7 \times 10^{-14}$ s and $j_h = 2.02$, $\tau_h = 1.3 \times 10^{-14}$ s. Then, knowing the relaxation times and using the classical expression $\mu_i = e\tau_i/m_i$ , we could estimate the electron and hole mobilities in our crystals as $\mu_e \sim 733\,\mathrm{cm^2/Vs}$ and $\mu_h \sim 31\,\mathrm{cm^2/Vs}$, respectively. The estimated values are in qualitative agreement with the measured Hall mobilities $\mu_e \sim 380\,\mathrm{cm^2/Vs}$ and $\mu_h \sim 26\,\mathrm{cm^2/Vs}$, for n-type and p-type crystals, respectively. From the values of the fitting parameter $j \sim 2$ for both types of carriers, we conclude that the dominant mechanism of scattering in our samples at RT is the scattering by optical phonons, in accordance with the results of electrical measurements.[14]

### 3.3 *ESR*

#### 3.3.1 *General observations*

ESR spectra in chalcopyrite-type compounds have been intensively studied especially in wide-gap I–III–$VI_2$ crystals such as $CuAlS_2$ and $CuGaS_2$. Most of the ESR studies are concerned with transition atom impurities which are known to be easily incorporated into the lattice as residual impurities which lead to coloration of crystals.[15] Of these transition atoms, Fe is known to be the dominant one, with Cr and Ni being second and third dominant contaminants, respectively. These elements are more easily incorporated into iodine-transport (IT) crystals than into melt-grown (MG) ones. The typical analyzed concentration of residual Fe impurity in IT crystal is about 100 ppm, whereas that in MG crystal is below the detection limit of the EPMA system (a few 10 ppm) and can be detected only by ESR measurements. These transition atoms are believed to be introduced from the source materials as well as from the environment during crystal growth experiments. Transition atoms are multivalent in semiconductors, which enables us to estimate the position of Fermi levels from ESR measurements. ESR is also known to be a powerful tool for detection of defects such as vacancies in semiconductors. We have already reported ESR signals related to the copper vacancy in $CuAlS_2$[16] and $CuAlSe_2$[17] crystals. In the present study we also utilize the ESR signal of defects to check the consistency of the Fermi level position and the defect states.

#### 3.3.2 *Assignment of signals*

The typical ESR spectra of the as-grown and annealed $CuInSe_2$ crystals are shown in Fig. 4. The spectrum of the as-grown sample exhibits a complex signal marked I, consisting of both isotropic and anisotropic components. The signal is centered on $g = 4.3$ and is believed to be originated from $Fe^{3+}$ in a strong noncubic ligand field. The Hamiltonian of the $Fe^{3+}$ ion ($^6S_{5/2}$) in the noncubic crystal field reads[18,19]

$$\mathcal{H} = g\beta \boldsymbol{H}\boldsymbol{S} + D\left(S_z^2 - \frac{1}{3}S(S+1)\right) + E(S_x^2 - S_y^2), \quad (10)$$

where $D$ and $E$ are parameters of the axial and rhombic components of the crystal field, respectively.

Both the axial and rhombic components of the ligand field cause the splitting of the sixfold-degenerate ground state $^6S_{5/2}$ of $Fe^{3+}$ into three Kramers doublets, resulting in the possibility of observing the ESR signal. The solutions of the above Hamiltonian depend on the parameter $E/D$ which describes the relative strength of the axial and rhombic terms of the crystal field. If $E \gg D$, we should observe a nearly isotropic signal around $g = 4.3$, which is in accordance with our results and has also been observed for $Fe^{3+}$–X pairs in $AgGaS_2$.[20] For the second limiting case, when $E \ll D$, we can expect an anisotropic signal consisting of several lines with $g$-values in the range 2–6, which has also been detected in our $CuInSe_2$ crystals.

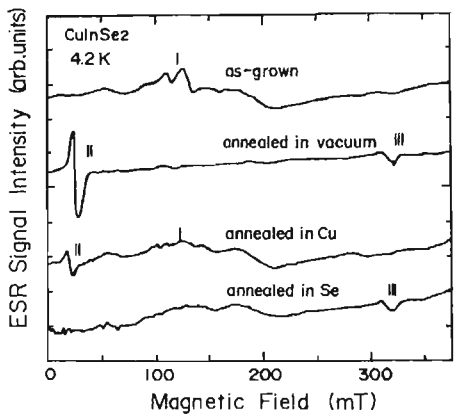


Fig. 4. ESR spectra of the as-grown and annealed $CuInSe_2$ crystals

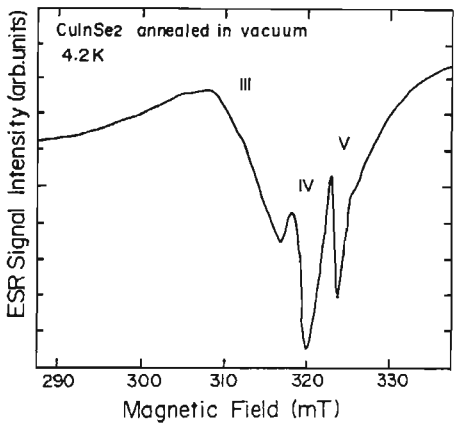


Fig. 5. Detailed ESR spectra of the vacuum-annealed samples, showing sharp IV- and V-signals superposed on a broader III-signal.

We believe, therefore, that the $Fe^{3+}$ ion in our samples forms two different complex defects of the type $Fe^{3+}$–X, one of which results in the strong axial field and the other, in the strong rhombic field of ligands on the site of $Fe^{3+}$ in the crystal lattice. Further studies are needed to elucidate the nature of the X-centers.

It can be seen from Fig. 4 that annealing the crystals in vacuum results in quenching of the $Fe^{3+}$ signal and in an appearance of four new signals: a highly anisotropic signal marked as II, and three isotropic signals marked III, IV and V, which are shown in detail in Fig. 5. Annealing in the presence of Cu partly quenches the $Fe^{3+}$-related signal and also leads to an appearance of the II-signal, whereas annealing in Se-vapor results in an appearance of the III-signal.

The highly anisotropic II-signal with the peak-to-peak linewidth $\Delta H_{pp} = 4$ mT, the effective $g$-factor of which takes its maximum value of $g_{eff//} = 28.7$ when the tetragonal $c$-axis of the crystal is set parallel to the external magnetic field, has also been observed in both $CuAlS_2$[21] and $CuInSe_2$[22] by other researchers, and has been attributed to the substitutional divalent iron impurity, the signal of which originates from the magnetically allowed microwave transitions $2 \Leftrightarrow -2$ within the lowest $M_s = \pm 2$ non-Kramers doublet.

The presence of $Fe^{2+}$ in vacuum-annealed crystals of $CuInSe_2$ was also confirmed by IR absorption spectra of highly compensated iodine-transport crystals, in which a broad absorption ranging between 2000 $cm^{-1}$ and 4500 $cm^{-1}$ with a peak around 3300 $cm^{-1}$ (0.41 eV) was observed and assigned to the crystal-field transition $^5E \Rightarrow {}^5T_2$ in the $3d^6$ manifold of $Fe^{2+}$ in $T_d$ symmetry.[23] This result provided the crystal-field parameter of approximately $Dq = 330$ $cm^{-1}$. However, such $Fe^{2+}$-originated absorption is not clearly resolved in the IR spectrum of the melt-grown crystal shown in Fig. 2(b). Subtraction of the free carrier absorption (dotted curve) from the experimental curve leads to the presence of a broad absorption band extending from 1000 $cm^{-1}$ to 7000 $cm^{-1}$. We believe that the $Fe^{2+}$-originated absorption is buried in the broad absorption band, since the total iron concentration in the melt-grown crystal is several orders of magnitude smaller than that in the IT crystal in which residual Fe concentration of as high as 0.01 at.% was detected.

The spectral position of the $Fe^{2+}$-originated absorption[23] was found to be close to that previously observed in other binary and ternary semiconductors, i.e., 2700 $cm^{-1}$ (ZnSe),[10] 3000 $cm^{-1}$ (CdS),[24] 3400 $cm^{-1}$ (ZnS),[25] 3200 $cm^{-1}$ ($CuGaS_2$)[26] and 3200 and 3900 $cm^{-1}$ ($CuInS_2$).[27] Crystal-field theory predicts the value of $g_{//}$ to be $g_e - 8k\lambda_o/10Dq$,[28] where $k$ is the covalency reduction factor and $g_e$ is the free-electron $g$-factor. Therefore, we can obtain the value of $g_{//}$ using the value of $Dq = 330$ $cm^{-1}$ from the IR absorption results. Using $k = 0.8$ and $\lambda_o = -100$ $cm^{-1}$ we obtain $g_{//} = 2.194$. Next, since under $\boldsymbol{H}//\boldsymbol{c}$ the resonance condition for the transition within the $M_s = \pm 2$ doublet is $(h\nu)^2 = (4g_{//}\beta H)^2 + \alpha^2$ (where $\alpha$ is the cubic field splitting parameter and $h\nu$ is the microwave energy),[28] we calculated the value of $\alpha$ from the known values of $g_{eff//}$ and $g_{//}$ using the expression

$$g_{eff//} = 4g_{//}\left[1 - \left(\frac{\alpha}{h\nu}\right)^2\right]^{-1/2}, \qquad (11)$$

and the obtained value of $\alpha$ was $|\alpha| = 0.28$ $cm^{-1}$, which is comparable to that for $CuAlS_2$,[21] where $|\alpha| = 0.45$ $cm^{-1}$. Further studies are necessary to obtain more convincing experimental evidence to correlate the ESR signal of $g_{eff} = 28.7$ with the IR absorption at 0.41 eV.

The isotropic III-signal with $g = 2.12$ and $\Delta H_{pp} = 10$ mT has been attributed to the signal from the hole trapped by the copper vacancy, and the signal is broadened by the hyperfine interaction with In nuclei (nuclear spin $I = 9/2$) in the second shell surrounding the $V_{Cu}$-defect. This signal is assigned on the basis of the reported results,[22,29] and is in agreement with the fact that this signal was observed only in Cu-deficient samples (vacuum- or Se-annealed) with $\Delta x < 0$ (see Table I).

Since the IV- and V-signals, shown in Fig. 5 and with isotropic $g$-factors of $g_{IV} = 2.023$ and $g_V = 2.002$, were observed only in the highly conductive n-type samples, they are believed to originate from electrons. We tentatively assign the IV-signal to electrons in a selenium-depleted phase of $CuIn_2Se_{3.5}$,[22] and the V-signal to electrons trapped by $In_{Cu}$-donors. The latter assignment is in agreement with the previously reported results,[29] as well as with the defect chemistry considerations, since, for the vacuum-annealed samples ($\Delta x < 0$), we can expect a high concentration of $In_{Cu}$-defects (Table I).

The narrowness of the IV- and V-signals ($\Delta H_{pp} \sim 0.5$ mT) indicates presence of exchange interaction effects and, therefore, a high concentration of donors, which is also in agreement with the IR absorption results, showing that our vacuum-annealed samples are degenerate n-type. It should be pointed out that neither of the IV- or V-signals could be attributed to free (mobile) electrons since, due to the large value of the spin-orbit splitting of the valence band on $CuInSe_2$, we expect the free-electron signal to be not around $g \sim 2$ (the case of conduction electrons in Si), but at a much smaller $g$-value of about 0.7.[30] However, we were not able to detect the signal with $g \sim 0.7$ in our experiment.

3.3.3 *Effect of the Fermi level motion*

The observed changes in the ESR spectra of the $CuInSe_2$ crystals, caused by thermal treatments in various atmospheres, can be explained by the annealing-induced motion of the Fermi level relative to the energy band edges.

It was determined from the IR absorption measurements that in the as-grown crystals the Fermi level is situated only about 80 meV above the top of the valence band and, hence, most probably below the $Fe^{2+}/Fe^{3+}$ demarcation level (Fig. 3(c), $E_{fp}$). Therefore, we could observe the $I$-signal from $Fe^{3+}$ in the ESR spectra of the as-grown samples.

Annealing in vacuum or Cu-atmosphere leads to the change of the conductivity type, wherein the samples are converted into the degenerate or semi-insulating n-type ones, respectively. These results indicate that the Fermi level is shifted upwards and is positioned inside the conduction band (vacuum-annealed samples, Fig. 3(a), $E_{fn}$) or in the midst of the band gap above the $Fe^{2+}/Fe^{3+}$ demarcation level (Cu-annealed samples, Fig. 3(b), $E'_{fn}$). Therefore, we observe the quenching of the $Fe^{3+}$ signal and an appearance of the II-signal from $Fe^{2+}$. Annealing in vacuum also results in a drastic increase in the concentration of the $V_{Cu}$- and $In_{Cu}$-defects (Table I), which leads to an appearance of the signals from carriers trapped by these defects.

Annealing in the Se-vapor results in a reverse process, wherein the Fermi level is shifted down towards the valence band (and below the $Fe^{2+}/Fe^{3+}$ demarcation level), which results in the highly conductive p-type conductivity and in the quenching of the ESR signal from $Fe^{2+}$.

It should be pointed out that the II-signal caused by $Fe^{2+}$ was found to be quenched to about one-half of its

original intensity upon illumination with infrared light (a 1.06 $\mu$m line of the YAG laser was used as an excitation source) in the semi-insulating n-type samples (Cu-annealed), but the degenerate n-type samples (vacuum-annealed) exhibit no changes of the signal under the same illumination. This phenomenon can be explained assuming that the $Fe^{+}/Fe^{2+}$ demarcation level is in resonance with the conduction band of $CuInSe_2$, i.e. lies inside of the conduction band (Fig. 3). Then, in the semi-insulating crystals, under IR light excitation some of the $Fe^{2+}$ ions capture electrons from the valence band and become monovalent, i.e. $Fe^{2+} + e^{-} \Rightarrow Fe^{+}$ , which results in the quenching of the $Fe^{2+}$ ESR signal. The last photo-ionization process, however, becomes impossible in degenerate n-type samples if the $Fe^{+}/Fe^{2+}$ demarcation level is situated below level $E_{en}$ (Fig. 3) in the conduction band, since electronic transitions to the completely filled states are impossible. Therefore, we believe that the $Fe^{+}/Fe^{2+}$ demarcation level is in resonance with the conduction band, in contrast to the $Fe^{2+}/Fe^{3+}$ demarcation level which is situated in the band gap of $CuInSe_2$.

## 4. Conclusions

We have studied the IR absorption and ESR spectra of the $CuInSe_2$ crystals in connection with the annealing-induced motion of the Fermi level relative to the energy band edges. The degenerate n-type crystals exhibited a free-electron absorption, whereas the p-type crystals showed both an inter-valence-band and a free-hole absorption, from the analysis of which the energy positions of the Fermi level have been evaluated, and the electrical parameters of the respective crystals have been estimated.

In the ESR spectra, the signals from $Fe^{2+}$ and $Fe^{3+}$ impurities, as well as those arising from native defects $V_{Cu}$ and $In_{Cu}$, have been detected, and the intensities of the ESR signals have been found to depend on the composition of the samples and the Fermi level position.

An important conclusion deduced from these results is that we can locally change the charged state of Fe impurity through appropriate control of the Fermi level, which indicates the possibility of realizing novel memory devices.


1) J. L. Shay and J. H. Wernick: *Ternary Chalcopyrite Semiconductors: Growth, Electronic Properties, and Application* (Pergamon, Oxford, 1975) p. 118.
2) I. Aksenov and K. Sato: Jpn. J. Appl. Phys. **31** (1992) 2352.
3) S. Endo, T. Irie and H. Nakanishi: Sol. Cells **16** (1986) 1.
4) J.A. Groenink and P.H.Janse: Z. Phys. Chem. **110** (1978) 17.
5) H. Neumann: Sol. Cells **16** (1986) 317.
6) W. Kaiser, R. J. Collins and H. Y. Fan: Phys. Rev. **91** (1953) 1380.
7) R. Braunstein and E. O. Kane: J. Phys. Chem. Solids **23** (1962) 1423.
8) H. Neumann, H. Sobotta, W. Kissinger, V. Riede and G. Kuhn: Phys. Status Solidi B **108** (1981) 483.
9) W. G. Spitzer and J. M. Whelan: Phys. Rev. **114** (1959) 59.
10) J. I. Pankove: *Optical Processes in Semiconductors* (Dover, NewYork, 1971) p. 129.
11) J. M. Baranowski, J. W. Allen and G. L. Pearson: Phys. Rev. **160** (1967) 627.
12) J. I. Pankove and E. K. Annavedder: J. Appl. Phys. **36** (1965) 3948.
13) S. Visvanathan: Phys. Rev. **120** (1960) 379.
14) S. M. Wasim: Sol. Cells **16** (1986) 289.
15) K. Sato and I. Aksenov: *Proc. 9th Int. Conf. Ternary and Multinary Compounds, Yokohama 1993*, Jpn. J. Appl. Phys. **32** (1993) Suppl. 32-3, p. 481.
16) I. Aksenov, N. Nishikawa and K. Sato: J. Appl. Phys. **74** (1993) 3811.
17) N. Nishikawa, T. Kai, I. Aksenov and K. Sato: Jpn. J. Appl. Phys. **34** (1995) L223.
18) W. C. Holton, M. de Wit, T. L. Estle, B. Discher and J. Schneider: Phys. Rev. **169** (1968) 359.
19) H. H. Wickman, M. P. Klien and Shirley: J. Chem. Phys. **42** (1965) 2113.
20) H. J. von Bardeleben, A. Goltzene, C. Schwab and R. S. Feigelson: Phys. Rev. B **5** (1980) 1757.
21) U. Kaufmann: Solid State Commun. **19** (1976) 213.
22) J. M. Tchapkui-Niat, A. Goltzene and C. Schwab: J. Phys. C: Solid State Phys. **15** (1982) 4671
23) K. Sato, I. Aksenov, N. Nishikawa, T. Shinzato and H. Nakanishi: to be published in *Proc. 10th Int. Conf. Ternary and Multinary Compounds, Stuttgart 1995*, J. Cryst. Res. Technol.
24) R. Pappalardo and R. E. Dietz: Phys. Rev. **123** (1961) 1188.
25) E. E. Vogel, O. Mualin, M. A. de Orue and J. Rivera-Iratchet: Phys. Rev. B **44** (1991) 1579.
26) K. Sato, H. Tsunoda and T. Teranishi: *Proc. 7th Int. Conf. Ternary and Multinary Compounds, Snowmass, 1986* (Mater. Res. Soc., Pittsburgh, 1987) p. 459.
27) N. Nishikawa, I. Aksenov, T. Shinzato, T. Sakamoto and K. Sato: Jpn. J. Appl. Phys. **34** (1995) L975.
28) A. Abraham and H. M. L. Pryce: Proc. R. Soc. London Ser. A **205** (1951) 135.
29) G. K. Padam, G. L. Malhotta and S. K. Gupta: Sol. Energy Mater. **22** (1991) 303.
30) L. M. Roth, B. Lax and S. Zwerdling: Phys. Rev. **114** (1959) 90.